Effects of nectin-3 misexpression on dendritic spine density during the postnatal development of layer 2/3 cortical neurons

Johanna Tomorsky[1,3], Philip R. L. Parker[1,3], Chris Q. Doe[1,2,3,4], Cristopher M. Niell[1,3]

[1]Institute of Neuroscience, [2] Institute of Molecular Biology, [3]Department of Biology, [4]Howard Hughes Medical Institute, University of Oregon, Eugene 97403

Address correspondence to:

Cris Niell, Institute of Neuroscience, Department of Biology, 1254 University of Oregon, Eugene, OR 97403. Email: cniell@uoregon.edu

Johanna Tomorsky, Stanford University, 318 Campus Drive, Stanford, CA, 94305, Email: jtomorsk@stanford.edu

Conflicts of interest

The authors report no conflicts of interest.

Funding sources

This work was supported by NIH grant numbers T32-HD007348 (JT), and DP2-EY023190 (CMN), and F32-EY027696 (PRLP), and by HHMI, where CQD is an Investigator.

Acknowledgements

The authors are grateful to Mandi Severson for her extensive work imaging dendrites and processing tissue for histological analysis. We would also like to acknowledge Emily Hill, Brynna Paros, Claire (Hoa) Bui, and Nathan Nguyen for their hard work processing tissue and counting dendritic spines. We are also very grateful to Judit Pungor for helping design the schematic for Figure 1A, and Nick Sattler and Rachel Lukowicz for their contributions to the project during their rotations in the Niell lab. We are also grateful to Bree Mohr for performing western blot analysis to determine nectin-3 knockdown.

Abstract

Developing cortical neurons must express numerous molecules to form and strengthen specific synaptic connections during circuit formation. Nectin-3 is a cell-adhesion molecule with known roles in the development and maintenance of hippocampal circuits. This protein and its binding partner, nectin-1, are selectively expressed in upper-layer neurons of mouse visual cortex, but their role in the development of cortical circuits is unknown. Here we block nectin-3 expression (via shRNA) or overexpress either full length (OE) or dominant-negative (DN, lacking a C-terminus) nectin-3 in developing layer 2/3 visual cortical neurons using *in utero* electroporation. We then assay dendritic spine densities at three developmental time points: eye opening (postnatal day (P)14), one week following eye opening after a period of heightened synaptogenesis (P21), and at the close of the critical period for ocular dominance plasticity (P35). shRNA knockdown of nectin-3 beginning at E15.5 or ~P19, increased dendritic spine densities at P21 or P35, respectively. Increasing nectin-3 binding/adhesion by expressing either DN nectin-3 (intact extracellular binding domain but lacking a C-terminus) or OE nectin-3 constructs beginning at E15.5, produced overall decreases in dendritic spine densities. However, DN nectin-3 expression alone prevented the increase in spine densities typically observed between P14 and P21. This suggests that nectin-3 intracellular signaling (reduced with DN expression) has a role in spine formation after eye opening. These data collectively suggest that both functional intracellular signaling and balanced overall expression of nectin-3 are required for normal synapse formation during the development of layer 2/3 visual cortical neurons.

Introduction

The development of mature brain circuits requires the selective formation, elimination, and strengthening of synaptic connections between neurons[1]. This process requires the timed expression and spatial localization of numerous molecules that are just beginning to be elucidated. Many studies

indicate that cell-adhesion molecules are involved in the formation and strengthening of synapses, though much is unknown about their specific roles in the maturation of various brain circuits[2]. The number and strength of synapses found on visual cortical neurons (often inferred from dendritic spine density and shape) depend on visual experience and developmental stage[3]. During the postnatal development of visual cortex, neurons experience an early increase in dendritic spine densities following eye opening[4,5]. This period of heightened synaptogenesis is followed by the critical period for ocular dominance plasticity (ODP, postnatal day (P)21-P35), which is associated with synaptic refinement and pruning[1,3,6,7]. Dendritic spine remodeling provides a mechanism for synapses to alter their strength and number based on experience, e.g. through activity-dependent synaptic plasticity, and is a critical component of normal cortical development[8]. Moreover, each cortical layer has a distinct timeline for the development of its unique visual response properties, likely a result of layer-specific synapse remodeling[9]. Here, we sought to characterize the role of the cell-adhesion molecule nectin-3 in spine density profiles in developing layer 2/3 (L2/3) visual cortical neurons.

The nectins are a group of immunoglobulin superfamily cell-adhesion molecules found to stabilize synapses at specialized structures called puncta adherentia junctions (PAJs)[10–13]. Transsynaptic nectins and cadherins, together with their intracellular signaling components at PAJs, help to form and remodel synapses over development (Figure 1A)[14,15]. For example, axonal (presynaptic) nectin-1 in dentate granule cells specifically binds to dendritic (postsynaptic) nectin-3 in CA3 principal neurons at the stratum lucidum in hippocampus to help guide and stabilize developing synaptic connections between these neurons (Figure 1A)[10,14]. Other studies have implicated nectins in a variety of biological and disease states, including long-term memory formation, stress, taopathy, and mental retardation, indicating that nectins may have different functions in the development, aging, and maintenance of various brain circuits[16–20]. While previous work suggests that nectin-1 and nectin-3 may be involved in

both the formation and maturation (stabilization) of synapses in hippocampus, their function in postnatal cortical development is unknown[14].

Here we identify a role for nectin-3 in the development of visual cortical neurons by examining dendritic spine densities after manipulating neuronal nectin-3 expression *in vivo*. Mammalian cortex has a conserved laminar structure, and nectin-1 and nectin-3 both have distinct upper layer expression patterns in postnatal mouse cortex[16,21,22]. The specific expression of nectin-3 in upper cortical layers may help facilitate the large developmental changes in visual response properties observed in this layer after eye opening relative to other layers (decreased firing rate and increased orientation selectivity)[9]. We assessed dendritic spine densities at three developmental time points (P14, P21, and P35) after *in utero* electroporation of nectin-3 shRNA, dominant-negative (DN), and overexpression (OE) constructs in developing mouse L2/3 visual cortical neurons. Nectin-3 knockdown by shRNA beginning at embryonic day (E)15.5 or ~P19[23], increased dendritic spine densities at P21 or P35, respectively. Unlike shRNA knockdown, the overexpression of either full-length or dominant-negative nectin-3 (beginning at E15.5), decreased dendritic spine densities overall. Since both dominant-negative and full-length nectin-3 constructs had intact extracellular binding domains, it follows that nectin-3 binding/adhesion may restrict synapse formation after eye opening. Alternatively, the expression of dominant-negative nectin-3, but not full-length nectin-3, prevented the increase in spine densities typically observed between P14 and P21. This suggests that when nectin-3 is present at synapses, nectin-3 intracellular signaling may facilitate spine formation at this time. The results of this study are consistent with a model where nectin-3 has roles in both the selective formation and selective removal of specific synapses in visual cortex during critical periods of development.

Materials and Methods

Immunohistochemistry

tdTomato fluorescence in electroporated neurons was amplified by immunohistochemistry (IHC) before imaging. Tissue preparation for IHC was performed as previously described [24]. Briefly, brains were perfused and then fixed overnight in 4% PFA (1 x PBS), after which brains were immersed in 30% sucrose (1 x PBS) for 24–48 hours. Brains were then sliced on a vibratome to a thickness of 80 µm, placed in cryoprotectent solution (30% sucrose, 1% polyvinyl-pyrrolidone, 30% ethylene glycol in 0.1 M PB), and stored at -20 ºC. IHC was performed on free floating sections as previously described [24]. Briefly, sections were washed 3 x 10 min in a 0.7% glycine solution (in PBS) and then blocked for 1–3 h in PBST (0.3% Triton-X in PBS) containing 5% goat and 5% donkey serum. Slices were then transferred to a primary antibody solution containing 1.5 µL/mL of rabbit anti-RFP (Rockland Cat# 600-401-379, RRID:AB_2209751) and incubated overnight at 4 ºC. The next day, slices were washed 1 x 10 min in PBST and then 3 x 10 min in PBS. Next, slices were transferred to a solution of 4 µL/mL of anti-rabbit Alexa Fluor 555 (Thermo Fisher Scientific Cat# A-21429, RRID:AB_2535850) secondary antibody in PBST and incubated at room temperature for 3 h. Slices were then washed for 10 min in PBST at room temperature, followed by an overnight wash in PBS at 4 ºC. The next day, slices were washed an additional 2 x 10 min in PBS, placed on slides, treated with DAPI (4′, 6-diamidino-2-phenylindole), and mounted with VECTASHIELD mounting media (Vector Labs).

In situ hybridization

The expression patterns of nectin-1 and nectin-3 were assayed by nonradioactive colorimetric RNA *in situ* hybridization, using solutions and probes as previously described [21,25–27]. Briefly, animals were perfused and brains were fixed overnight in 4% PFA and then cryoprotected in a 30% sucrose solution. Brains were then cryosectioned to a thickness of 30 µm, mounted on Superfrost Plus slides

(Fisherbrand), and stored at -80 °C until use. 30 µm sections were brought to room temperature, washed in PBS and acetylated[27]. Slides were then pre-hybridized in hybridization solution in a humidity chamber for 2 h at 70 °C. The riboprobes to *Pvrl1* and *Pvrl3* (the genes encoding nectin-1 and nectin-3 proteins) were generated with dig-labeled nucleotides and SP6 RNA polymerase using probe sequences and protocols described by the Allen Brain Institute[22,27,28]. Riboprobes were diluted in hybridization solution to a concentration of 1–2 ng/µL, and slides were hybridized overnight at 70 °C with each probe. Slides were then washed (at 70 °C) and blocked before incubating overnight at 4 °C in anti-dig sheep Fab fragments conjugated to alkaline phosphatase (AP; Roche No. 11093274910) diluted 1:2500 in blocking solution. Slices were then washed at room temperature with MABT buffer and then AP staining buffer, after which 3.5 µL/mL NBT, 2.6 µL/mL BCIP, and 80 µL/mL levamisole in AP staining buffer was applied. The AP colorimetric reaction was observed closely as it developed for 3–48 h at 37 °C and was stopped by washing twice with PBS (0.1% Tween-20) and twice with deionized H_2O. Slides were then dehydrated in graded ethanols and mounted using Permount Mounting Medium (Fisher).

Design of Cre-dependent shRNA plasmids for *in utero* electroporation

Nectin-3 shRNA constructs were designed using previously published siRNA sequences[29]. These 19 bp sequences were used to design shRNA hairpin sequences for cloning into a pSico vector[29,30]. The nectin-3 and scramble shRNA oligos used for cloning were as follows:

Pvrl3 shRNA1 sense oligo:

TGGCCGGATTCTTTAATTGATTCAAGAGTCAATTAAAGAATCCGGCCTTTTTTC

Pvrl3 shRNA1 antisense oligo:

TCGAGAAAAAAGGCCGGATTCTTTAATTGACTCTTGAATCAATTAAAGAATCCGGCC A

Pvrl3 shRNA2 sense oligo:

TGTTTATTGGCGTCAGATAATTCAAGAGATTATCTGACGCCAATAAACTTTTTTC

Pvrl3 shRNA2 antisense oligo:

TCGAGAAAAAAGTTTATTGGCGTCAGATAATCTCTTGAATTATCTGACGCCAATAAACA

Scr sense oligo:

TGCTACACTATCGAGCAATTTTCAAGAGAAATTGCTCGATAGTGTAGCTTTTTTC

Scr antisense oligo:

TCGAGAAAAAAGCTACACTATCGAGCAATTTCTCTTGAAAATTGCTCGATAGTGTAGCA

Cloning into pSico was modified from methods previously described[30]. Briefly, restriction enzymes XhoI and HpaI were used to digest the pSico vector (Addgene plasmid #11578). Digested vector RNA was then dephosphorylated using shrimp alkaline phosphatase (Roche) for 60 min at 37 °C to prevent re-ligation of the vector, followed by deactivation at 65 °C for 15 min. 1 µL of 100 µM sense and antisense shRNA oligos (synthesized by IDT) were then annealed and phosphorylated using T4 PNK (1µL 10X T4 Ligation Buffer (NEB), 6.5 µL H2O, and 0.5 µL T4 PNK (NEB)). Annealing was performed in a thermocycler at 37 °C for 30 min and then 95 °C for 5 min, followed by a ramp down to 25 °C at 5 °C/min. Vector and insert were the ligated with Quick Ligase (NEB) using manufacturers protocols. Ligated plasmid was then treated with PlasmidSafe exonuclease (Lucigen), to prevent unwanted recombination products, and used to transform NEB Stable Competent *e. coli*. Positive colonies were grown in LB + amp., after which plasmid DNA was extracted (QIAprep Spin Miniprep Kit) and sequenced using the pSico sequencing primer: CAAACACAGTGCACACAACGC [30]. Plasmid DNA verified to contain the shRNA insert was then prepped for electroporation from 200–400 µL of cultured *e. coli* using a NucleoBond Midi or Maxi EF kit (Clontech) and eluted to a concentration of 5–10 µg/µL in TE.

Expression constructs for *in utero* electroporation

A nectin-3 overexpression construct was created by modifying a pCag-iCre expression vector (Addgene plasmid # 89573). Nectin-3 alpha was PCR amplified (KOD hot start DNA polymerase, Sigma-Aldrich) from a mouse brain cDNA library using the forward primer: GTTGAGGACACGCGCG and reverse primer: CTGTTAGACATACCACTCCCTCC. Amplified DNA was run on a gel and a band the length of nectin-3 (~1800bp) was cut from the gel and purified (Qiaquick Gel Extraction Kit, Qiagen). Sequences were then amplified (KOD hot start DNA polymerase) using nested primers with and without a FLAG-tag and containing restriction sites for MluI and Not1. Primer sequences were as follows:

Nectin-3 F: TAAGCA-ACGCGT-GCCACCATGGCGCGGACCCCG

Nectin-3 R: TGCTTA-GCGGCCGC-TTA-GACATACCACTCCCTCCTG

Nectin-3 R Flag: TAAGCA-GCGGCCGC-TTA-CTTGTCGTCATCGTCTTTGTAGTC-GACATACCACTCCCTCCTG

Amplified DNA was then gel purified and digested using the same restriction sites. The pCAG-iCre plasmid was also digested with MluI and NotI to remove the iCre sequence from the vector. Digested vector and nectin-3 were then ligated, used to transform *e. coli*, and prepped for electroporation (NucleoBond Midi or Maxi EF kit, Clontech). Positive clones were sequenced using pCag F: GCAACGTTGCTGGTTATTGT, and Bglob-pA R: TTTTTGGCAGAGGGAAAAGAT sequencing primers.

A previously published dominant-negative construct for nectin-3 was kindly gifted by Dr. Gil-Sanz and Dr. Mueller [29]. FLEX-tdTomato constructs (plasmid #51509 and #51505) and the Cre-expression plasmid (plasmid #51904) were obtained from Addgene.

Western blot analysis of overexpression and shRNA constructs

The newly designed nectin-3 overexpression construct was transfected (Lipofectamine Reagent, Thermo Fisher Scientific) into HEK-293 cells using manufacturer's protocols. A western blot was then run using 10 ug of protein extracted from transfected cells, as previously described[31]. When stained with an anti-nectin-3 antibody (Abcam Cat# ab63931, RRID:AB_1142394) western blot analysis showed greatly increased expression compared to endogenous HEK-293 expression (Figure 5B). The western blot was also stained with an alpha-tubulin antibody (Sigma-Aldrich Cat# T9026, RRID:AB_477593) to ensure similar overall protein levels between conditions. To determine whether the newly designed shRNA constructs were effective, we co-transfected nectin-3 overexpression and shRNA plasmids into HEK293 cells. To test the efficacy of co-transfection in HEK-293 cells, lipofectamine was used to co-transfect GFP and RFP expressing constructs using manufacturers protocols. Using a 4:3 ratio of GFP to RFP, nearly 100% co-transfection was observed (data not shown). pSico nectin-3 and scramble-shRNA constructs were then altered to artificially replicate Cre-excision using site-directed mutagenesis (Q5 site directed mutagenesis kit: New England Biolabs). The GFP-stop sequence and one loxP site were removed from pSico by site directed mutagenesis using the following primers: F: CGCATAACTTCGTATAGTATAAATTA, R: AATTACTTTACAGTTAGGGTGAG. The new nectin-3 shRNA and scramble shRNA plasmids did not require Cre for expression and were co-transfected into HEK-293 cells with the nectin-3 overexpression construct at a 4:3 ratio. Again, 10 ug of extracted protein was loaded onto a gel for western blot, and the blot was stained using nectin-3 and alpha-tubulin antibodies. Due to the high levels of nectin-3 expression from the overexpression construct, nectin-3 levels were much higher than alpha-tubulin. For this reason, images of the bands needed to be adjusted individually to bring each into dynamic range. Band intensities were then quantified using image-j, and nectin-3 band intensities were normalized to a-tubulin intensity. This provided an expression index for

each condition which showed reduced expression of nectin-3 when nectin-3 specific shRNA was present as compared to the scramble control (Figure 2B).

***In utero* electroporation of plasmid DNA**

All experimental protocols were approved by the University of Oregon Institutional Animal Care and Use Committees, in compliance with the National Institutes of Health guidelines for the care and use of experimental animals. *In utero* electroporation was performed at E15.5 to target L2/3 pyramidal neurons, as previously described[32,33]. For shRNA knockdown using pSico, a solution of 2 µg/µL pSico-shRNA plasmid, 1.5 µg/µL FLEX-tdTomato plasmid, and 0.02 µg/µL Cre-expression plasmid was prepared in PBS (pH 7.2 for injections). In addition, 0.1% Fast Green dye was used to visualize plasmid DNA as it entered the ventricle with injection. For overexpression (OE) and dominant-negative (DN) experiments, a solution of 0.5 µg/µL DN or OE expression vector, 1ug/µL FLEX-tdTomato plasmid, and 0.01 µg/µL Cre-expression plasmid was prepared in PBS and 0.1% Fast Green.

Timed pregnancies were set up overnight between a hybrid strain of WT female mice (F1 cross of C57BL/6J and 129S1/SvlmJ, Jax) and either the same strain of WT male mice or *CaMKII-Cre* homozygous transgenic male mice (Jax 005359). The day the plug was observed was designated embryonic day 0.5 (E0.5). 15.5-day pregnant mice were anesthetized with 2% isofluorane (0.8% O_2) for the duration of the surgery. A small incision was made in the abdomen of pregnant females and the uterus was pulled out of the abdominal cavity. Approximately 1 µL of plasmid solution was injected through the uterus and scull into the lateral ventricle of E15.5 embryos[33]. Visual cortex was then targeted with an electrical pulse through tweezer-type electrodes using five, 45 V, 100 ms pulses at a 1 s interval. The uterus was then placed back in the abdominal cavity, the mouse was sutured, and allowed to recover. Animal health was monitored daily after surgery until pups were born (~4 days later).

Electroporated mice were perfused as previously described[24] at P14, P21, or P35, and brains were prepared for immunohistochemistry.

Microscopy and spine counting

In situ hybridizations were imaged using an EC Plan-NEOFLUAR 5x/0.16 objective on a Zeiss Axio Imager.A2 wide field epifluorescence microscope having an X-Cite 120Q LED excitation lamp and a Zeiss AxioCam MRm 1.4-megapixel camera. ZEN lite imaging software (2012) was used to view images, and Adobe Photoshop CS6 was used for background removal and color processing of images.

Coronal sections of electroporated brain tissue were checked for fluorescent neurons in V1 using the Zeiss Axio Imager.A2 microscope and an EC Plan-NEOFLUAR 2.5x/0.085 objective. Immunohistochemistry was performed on sections confirmed to have electroporated cells. The location of electroporated neurons was determined using DAPI staining and a mouse brain atlas[34]. Neurons located V1 L2/3 were imaged on a ZeissLSM700 confocal microscope using Zen software. Images of secondary (at least one branch away from the soma) apical and basal dendrites were analyzed. Secondary apical dendrites directly extending laterally from the primary apical dendrite were preferentially selected (as opposed to apical tufts). High resolution images of dendrites for spine counting were taken using a Plan-Apochromat 63x/1.40 Oil DIC objective with 1.1–1.3x zoom, a speed of 8, averaging of 2, z-resolution of 0.3 µm, and variable laser intensities to capture dendritic spines. Spines in high resolution images of dendrites were counted manually using the open source FIJI image analysis software and the multipoint tool. Neurite lengths were measured using the 'simple neurite tracer' plugin.

Statistical analysis

Linear mixed models were used to model all data with the 'lme4' package in R. For models having multiple comparisons, a Tukey's post-hoc test was applied in R using the 'emmeans' package

and the Kenward-Rodger method to determine degrees of freedom. For models having a single comparison, a type III ANOVA was applied using the 'car' package to determine P-values. Overall differences in dendritic spine densities between control (scramble shRNA) and either Nec3-shRNA (Figure 2), Nec3-DN (Figure 4), or Nec3-OE (Figure 5) conditions were determined using the following linear mixed model in R:

*lmer (Density ~ Condition*Age + Apical_Basal + (1|Animal) + (1|Animal:Cell_number))*

In this model, Condition and Age are interacting fixed effects, and whether the dendrite was apical or basal is added as an additional fixed effect. 3-4 animals were analyzed per condition, and in these experiments, apical and basal dendrites were often obtained from the same cell. For this reason, both animal and cell number were added as random effects, and cell number is nested within animal. Tukey's post hoc test was then used to determine overall pairwise differences between conditions.

Differences in dendritic spine densities between P14 and P21 or P21 and P35 for each condition were modeled individually using the same linear mixed model shown above but removing Condition as a fixed effect (Figures 3, 4, 5, 6). P14-P21 and P21-P35 data were analyzed separately. Similarly, differences in dendritic spine densities between control and either Nec3-shRNA (Figure 2), Nec3-DN (Figure 4), or Nec3-OE (Figure 5) conditions at each age were modeled individually using the same linear mixed model but removing Age as a fixed effect. A type III ANOVA was then applied to test for differences between groups.

The same model was used in Figure 6B to estimate overall developmental trajectories of dendritic spine densities by combining Nec3-shRNA, Nec3-OE, and control conditions in a single analysis (Nec3-DN showed no developmental changes in dendritic spine densities so was removed from this analysis). This model was then modified to examine Basal (Figure 6C) or Apical (Figure 6D) dendrites separately for developmental changes in dendritic spine densities. For this analysis, we

removed Apical_Basal as a fixed effect, and Cell_number as a random effect (only one apical or basal dendrite was sampled per cell):

*lmer (Density ~ Condition*Age + (1|Animal))*

This modified model was then used to estimate overall developmental trajectories of apical and basal dendritic spine densities separately by combining Nec3-shRNA, Nec3-OE, and control conditions in a single analysis (as with combined data in Figure 6B, Nec3-DN was removed from this analysis). Apical and basal dendrites were also analyzed separately to determine differences in dendritic spine densities between ages for each individual condition. For these analyses, the modified model was applied to data from a specific condition and Condition was removed as a fixed effect (Figure 6C, D). Finally, we examined Apical and Basal dendrites separately for differences between conditions at each age. For these analyses, the modified model was applied to data from a specific age group, and 'Age' was removed as a fixed effect. Tukey's post-hoc test was then used to determine differences between conditions and ages (Figure 6, Supplemental Table 1).

For the comparison of Nec3-shRNA and control data from CaMKII animals at P35 (Figure 3), the following model was used followed by a type III ANOVA test:

lmer (Density ~ Condition + Apical_Basal + (1|Animal))

Apical and basal dendrites were sampled from different cells in this experiment, so cell number was not added as a random effect.

Finally, in Supplemental Figure 1, we analyzed data from a single time point for differences between all conditions. For this analysis, the original statistical model was used but 'Age' was removed as a fixed effect. Tukey's post-hoc test was then applied, as described above. Select P-values from these analyses are summarized in Supplemental Table 1.

Results

Nectin-3 and nectin-1 are expressed in upper layers of visual cortex.

Previous studies have shown a role for nectin-3 and its binding partner nectin-1 in the formation and maintenance of hippocampal synapses (Figure 1A)[10,12,14]. To gain insight into the role of nectin-3 in developing visual cortex, we first determined by *in situ* hybridization (ISH) that the expression of both nectin-3 and its binding partner, nectin-1, were enriched in L2/3 cortical neurons just after eye opening (P16; Figure 1B). This confirmed ISH data found at Allen Brain Atlas, showing enriched L2/3 expression of both nectins beginning in late-embryonic/early-postnatal development and continuing through adulthood[22]. Since the expression of both nectins was enriched in upper layers of cortex, we sought to specifically manipulate the expression of nectin-3 in developing L2/3 cortical neurons. To accomplish this, we used *in utero* electroporation, a technique allowing the cell type-specific incorporation of plasmid DNA into developing cortical neurons, depending on the time of manipulation.

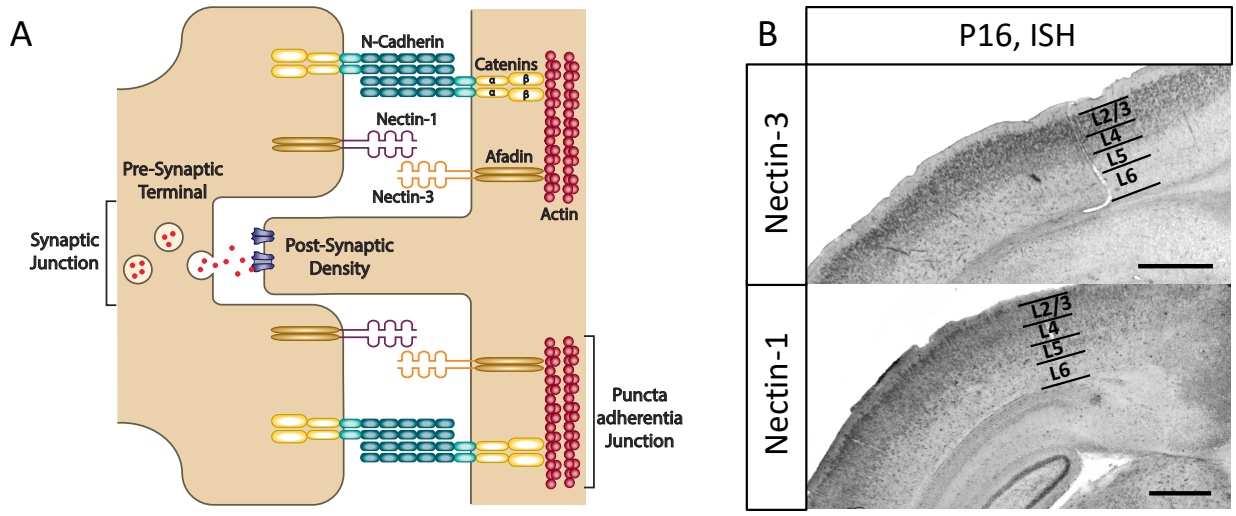

Figure 1. Model of nectin-3 and nectin-1 interaction from hippocampal synapses, and expression in upper layers of visual cortex.
(A) Nectin-1 and nectin-3 have been shown to bind at puncta adherentia junctions (PAJs) in hippocampus and interact with actin secondarily through their binding partner afadin[10,12,14]. Nectin and afadin have also been shown to interact with N-cadherin at PAJs[10,11,14,35]. N-cadherin binds β-catenin,

which in turn binds α-catenin, which associates with afadin to co-localize nectins and cadherins[11–13]. PAJs are found at synapses and are stabilizing sites of adhesion between axons and dendrites. PAJs are distinct from synaptic junctions (SJs), which are the sites of neurotransmission. SJs incorporate neurotransmitter receptors at post-synaptic densities on dendritic spines, and synaptic vesicles at presynaptic active zones[12,14].
(B) *In situ* hybridizations (ISH) to nectin-3 and nectin-1 demonstrate enriched expression in upper cortical layer neurons in V1 at P16 (5x objective, scale bar = 500 μm).

shRNA knockdown of nectin-3 at E15.5 yields an overproduction of spines at P21

To knockdown nectin-3 in developing neurons *in vivo*, we first designed new plasmid vectors to express nectin-3 short-hairpin RNA (shRNA) or scrambled control shRNA (Figure 2A). We used previously published siRNA sequences[29] to design our nectin-3 shRNA constructs and cloned these hairpins into the Cre-dependent pSico vector (Addgene plasmid #11578) [30]. When a nectin-3 expression construct was co-transfected into HEK-293 cells with our new nectin-3 shRNA constructs (with the floxed GFP-Stop sequence removed, see Methods), nectin-3 protein was reduced compared to cells co-transfected with a scrambled shRNA construct (Figure 2B). This is consistent with previously published data showing nectin-3 was knocked down in cultured cortical neurons using the same siRNA sequences[29].

We used *in utero* electroporation to introduce either or both nectin-3 shRNA1 and shRNA2 or a scrambled shRNA (Figure 2A, B) to developing L2/3 cortical neurons at E15.5 (Figure 2D). shRNA constructs were co-electroporated with a Cre-dependent tdTomato construct and a low concentration of a pCag-Cre plasmid (Figure 2A). We identified tdTomato expressing neurons in L2/3 of primary visual cortex (V1) and assayed both apical and basal dendrites to determine significant changes in dendritic spine densities (Figure 2C). We assayed dendritic spine densities at three developmental time points: eye opening (P14), one week after eye opening (P21), and at the close of the critical period for ocular dominance plasticity (P35; Figure 2D). This allowed us to assess nectin-3 function during critical

periods in the development of visual cortex for synapse formation (P14-P21)[4], as well as synaptic refinement (P21-P35)[7,36,37].

Knocking down nectin-3 at E15.5 significantly impacted dendritic spine densities during postnatal development. Neurons electroporated with either scrambled shRNA (control) or nectin-3 shRNA constructs showed an increase in spine densities between P14 and P21, consistent with previous reports of spinogenesis following eye opening in visual cortex (Figure 2E)[4]. However, nectin-3 knockdown amplified this change, yielding significantly higher spine densities than control at P21 (Figure 2E). By P35, the dendritic spine densities of Nec3-shRNA neurons were no longer significantly different from control neurons. This result indicates that the knockdown of nectin-3 at E15.5 may have increased synaptic pruning between P21 and P35, though Nec3-shRNA dendritic spine densities are not significantly different between these two time points. Collectively, these results are consistent with a model where the extended knockdown of nectin-3 leads to an overproduction of weak spines after eye opening, which are readily pruned over the critical period for ocular dominance plasticity (P21-P35) due to reduced spine stability.

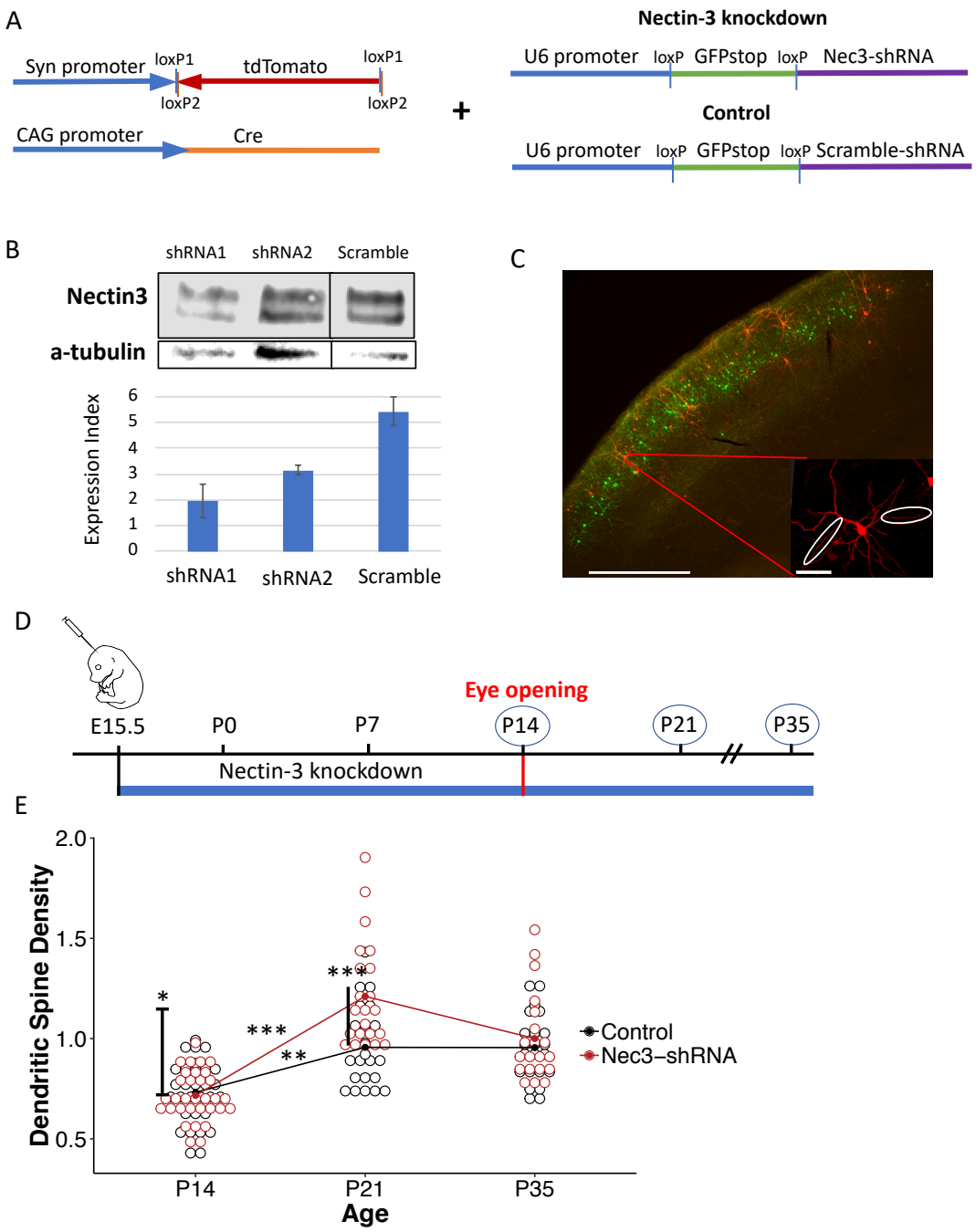

Figure 2: Nectin-3 knockdown at E15.5 yields an overproduction of spines at P21
(A) A Cre-expression plasmid was co-electroporated with a Cre-dependent FLEX tdTomato construct and Cre-dependent shRNA constructs. For shRNA knockdown, Cre-dependent shRNA constructs to nectin-3 were used containing a loxP flanked GFP-stop sequence to prevent the expression of shRNA in the absence of Cre. As a control, a scramble shRNA construct was designed using the same vector.
(B) Western blot showing nectin-3 expression in HEK-293 cells after co-transfection of a nectin-3 expression plasmid with either nectin-3 or scramble shRNA constructs (Cre-excised, see methods). The images of nectin-3 and α-tubulin bands were adjusted to observe band specific dynamic ranges. Relative

expression levels were quantified after image analysis using an expression index for nectin-3 expression normalized to α-tubulin. Expression was decreased for both nectin-3 shRNA constructs tested as compared to scramble shRNA (technical replicates, N = 2).
(C) 10x image of neurons electroporated with a pSico shRNA construct at P21 in visual cortex. Cre-positive tdTomato-expressing cells assumed positive for shRNA expression can be observed surrounded by Cre-negative GFP-expressing cells. All cells migrated normally to L2/3 (scale bar = 500 µm). Inset: Neurons were chosen in V1 (40x image, scale bar = 50 µm), and apical and basal dendrites, at least one branch away from the soma, were imaged at 63x for spine counting.
(D) Dendritic spine densities were measured at three time points: eye opening (P14), one week after eye opening (P21), or at the closing of the critical period for ODP (P35).
(E) Differences in dendritic spine densities between neurons electroporated at E15.5 with a scrambled control shRNA or shRNA to nectin-3. Densities were assayed at P14, P21, and P35, and apical and basal dendrites are pooled. Significance is denoted by '*', and P-values are listed in Supplemental Table 1. A significant overall difference between conditions was observed when all time points were included in a single model (P = 0.0489). Significant differences between conditions at P21 (P = 0.0003) and between time points (control P14-P21; P = 0.003, and Nec-3 shRNA P14-P21; P = <0.0001) are also shown.

Nectin-3 knockdown from P14 onwards increases dendritic spine densities at P35

Early (E15.5) shRNA knockdown of nectin-3 yielded an overproduction of dendritic spines after eye opening, significantly increasing dendritic spine densities at P21 relative to control. On the other hand, dendritic spine densities between Nec3-shRNA and control neurons were not different at P35, indicating that the extra spines produced at P21 may have been removed over the critical period for ODP. We next wanted to test whether the initial overproduction of spines at P21 may have led to compensatory pruning by selectively knocking down nectin-3 later in development. For this experiment, we co-electroporated the same Cre-dependent Nec3-shRNA constructs (or control scramble shRNA) and a Cre-dependent tdTomato construct into transgenic *CaMKII-Cre* mice at E15.5 (Figure 3A, C). In a previous study of *CaMKII-Cre* mice, Cre/loxP recombination was first observed in cortex and hippocampus at P19 and expression was described as robust by P23[23]. Both apical and basal dendritic spine densities were analyzed at P35, to allow time for full shRNA expression and knockdown of nectin-3 in L2/3 cortical neurons (Figure 3B, C). Unlike early (E15.5) shRNA knockdown of nectin-3, late (~P19) nectin-3 knockdown significantly increased dendritic spine densities at P35 relative to control

(Figure 3D). This increase in spine density was not specific to apical or basal dendrites (Figure 3D, Supplemental Table 1). From this we conclude that nectin-3 may also facilitate pruning over the critical period for ODP.

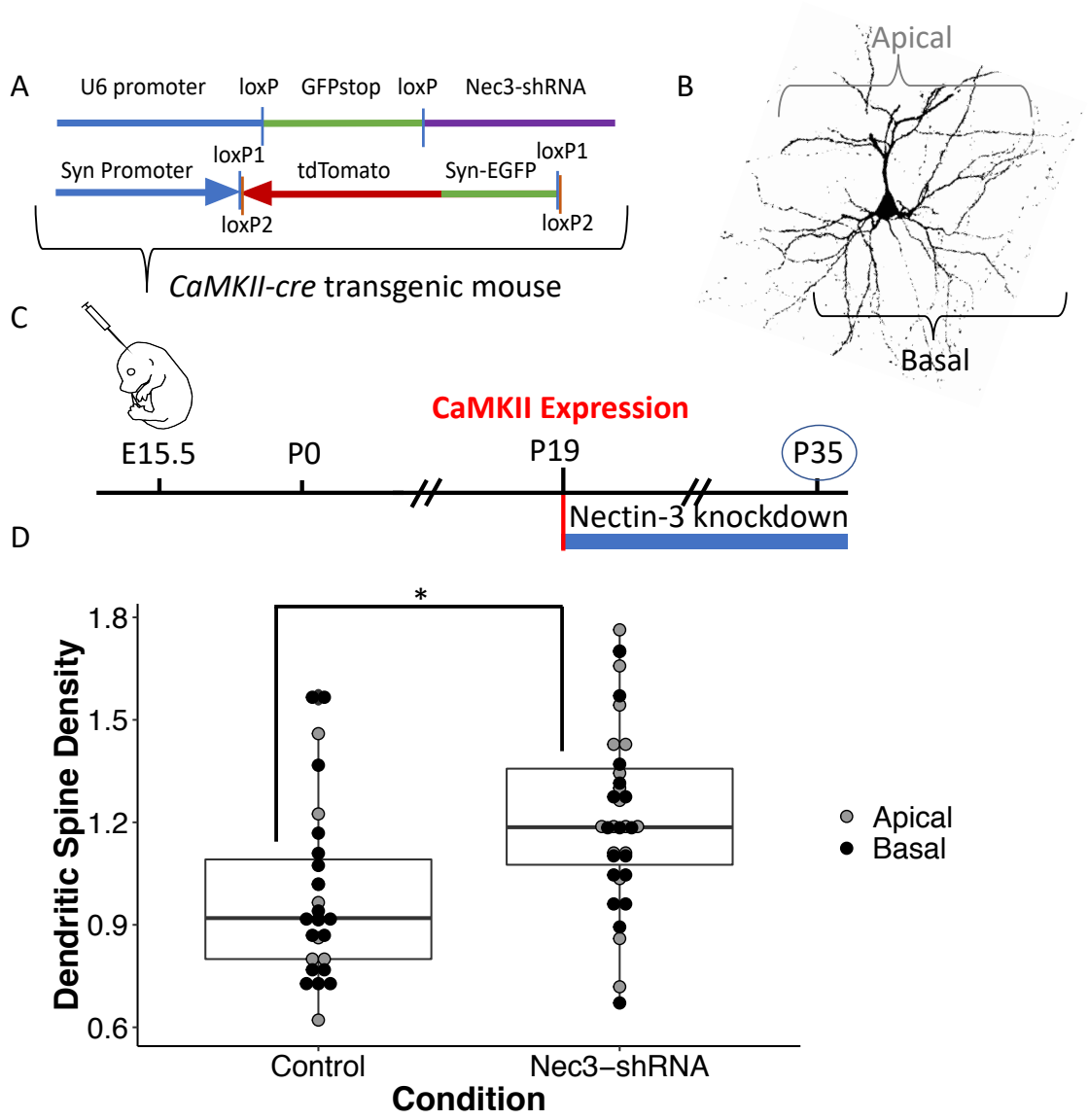

Figure 3. Nectin-3 knockdown after P14 increases dendritic spine densities at P35.
(A) A Cre-dependent shRNA construct to nectin-3 (or scramble shRNA construct) was co-electroporated with a Cre-dependent FLEX tdTomato plasmid (also expressing synaptophysin-EGFP) into developing CaMKII-Cre transgenic mice.
(B) Both apical and basal dendrites on CaMKII-Cre/shRNA/tdTomato positive neurons were imaged at P35 (40x image).

(C) Mice were electroporated at E15.5 to target developing L2/3 neurons, but Cre recombination is not observed until ~P19 in the CaMKII-Cre mouse line used[23]. For this experiment, neurons develop normally until nectin-3 knockdown at ~P19. Mice were sacrificed and neurons were imaged at P35. (D) Dendritic spine densities are significantly higher at P35 (P = 0.0123) when nectin-3 is knocked down at ~P19 using a CaMKII-Cre mouse. Apical (grey dot) and basal (black dot) dendrites were similarly affected (P = 0.2745). Significance is denoted by '*', and P-values are listed in Supplemental Table 1.

Expression of dominant-negative nectin-3 prevents normal spinogenesis after eye opening

The shRNA knockdown of nectin-3 likely reduces synaptic adhesion over development, which other studies have suggested may increase synapse number, perhaps to compensate for decreased synapse strength[14,38]. Neurons may also compensate for the removal of this synaptic component by overexpressing other functionally similar molecules[38,39]. As an alternative method of blocking nectin-3 signaling in developing neurons, we overexpressed a dominant-negative nectin-3, retaining its extracellular binding domain but lacking its C-terminus. Dominant-negative nectin-3 expression should competitively exclude endogenous nectin-3 from synapses and prevent nectin-3 intracellular signaling, but not extracellular binding[29,40]. We used *in utero* electroporation to express a dominant-negative nectin-3 construct in developing L2/3 neurons beginning at E15.5 (Figure 4C). The dendritic spine densities of apical and basal dendrites were then assayed at P14, P21, and P35 (Figure 4B, C).

Dominant-negative nectin-3 expression had a very different effect on postnatal dendritic spine densities compared to nectin-3 shRNA expression. Nec3-DN produced an overall decrease in spine densities compared to control (scramble shRNA) and prevented the increase in spine densities typically observed between P14 and P21 (Figure 4D). Since dominant-negative nectin-3 had an intact extracellular binding domain, it is possible that the adhesive properties of nectin-3 were left intact, and high overall cellular adhesion restricts spine formation after eye opening. This could potentially explain why Nec3-shRNA increased spine densities (decreased adhesion) and Nec3-DN decreased spine densities (increased adhesion, no signaling). Furthermore, previous studies have shown the C-terminus

of nectin-3 interacts with the actin cytoskeleton through afadin, recruits N-cadherin, and signals through Rac1 and Cdc42 pathways[10,14,41–44] (Figure 1A). These intracellular signaling mechanisms have known functions in synapse formation[45,46]. These results are consistent with a model where the adhesive properties of nectin-3 are restrictive to synapse formation after eye opening, while intracellular signaling by nectin-3 facilitates synapse formation. Further studies are necessary to determine why the two methods of blocking nectin-3 (shRNA vs. dominant-negative expression) produced different results.

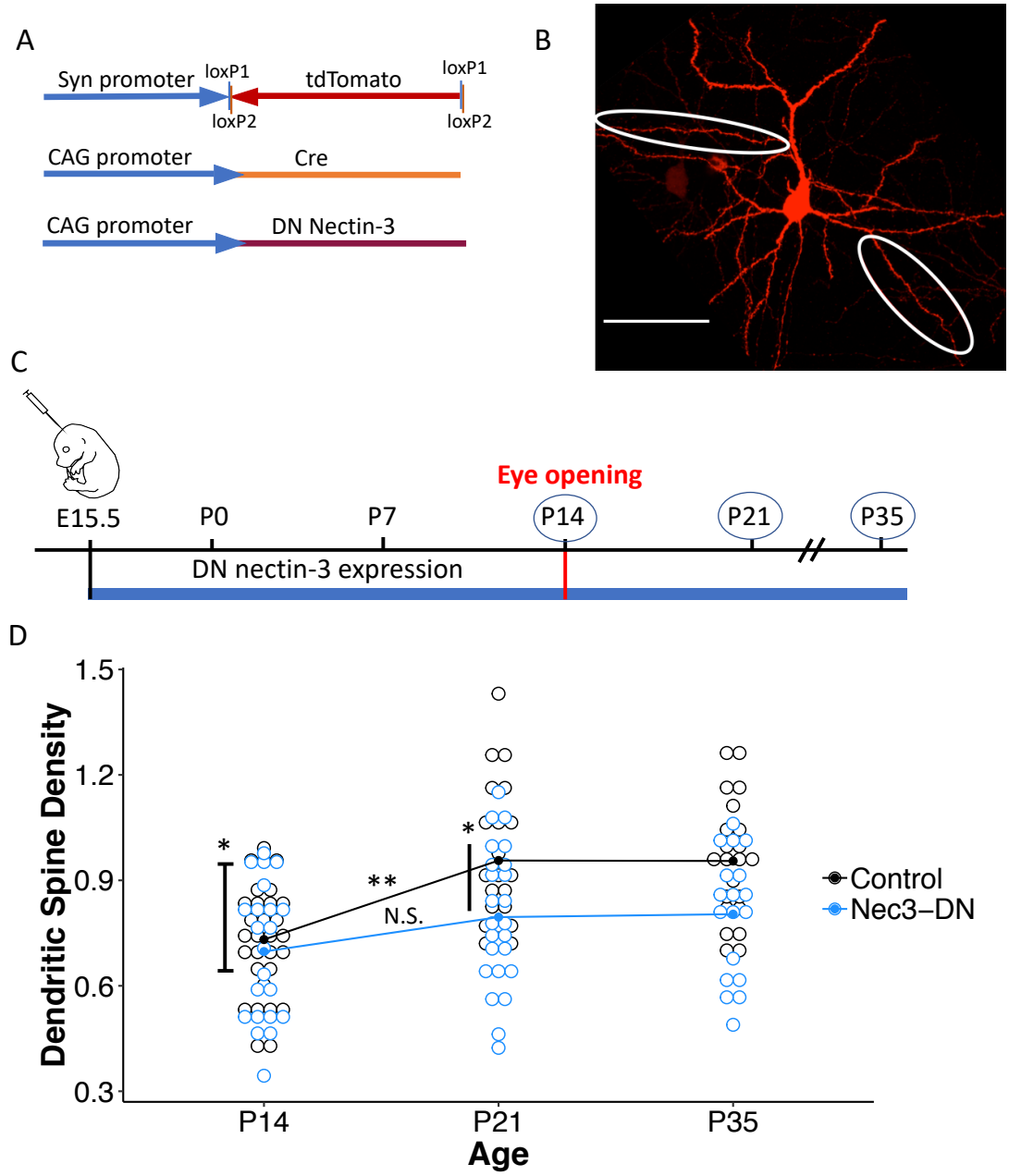

Figure 4: Dominant-negative nectin-3 at E15.5 expression restricts spine formation after eye opening
(A) To block nectin-3 signaling in developing L2/3 neurons, a construct driving the expression of dominant-negative (DN, lacking cytoplasmic tail) nectin-3 was co-electroporated with a Cre-dependent tdTomato construct and a Cre-expression plasmid.
(B) Representative image of an electroporated neuron with select apical and basal dendrites circled (scale bar = 50 µm).
(C) Dominant-negative nectin-3 constructs were introduced to L2/3 cortical neurons by *in utero* electroporation at E15.5. Dendritic spine densities were measured at P14, P21 or P35.
(D) Dominant-negative nectin-3 expression produced an overall decrease in dendritic spine densities compared to control (scramble shRNA) neurons when all time points were considered (P = 0.0364). A significant decrease in dendritic spine densities was also observed at P21 (P = 0.0136) when data from each age was analyzed separately. In addition, spine densities did not increase between P14 and P21 (P = 0.3312). Apical and basal dendrites are pooled in this analysis. Significance is denoted by '*', and P-values are listed in Supplemental Table 1.

Overexpression of nectin-3 at E15.5 decreases dendritic spine densities, but preserves the developmental increase in spine densities between P14 and P21

We next examined the effect of overexpressing full-length nectin-3 in L2/3 neurons over development. A newly designed nectin-3 expression plasmid (Figure 5A) was shown to dramatically increase nectin-3 expression after transfection into HEK-293 cells (Figure 5B). This nectin-3 overexpression construct was electroporated at E15.5, and apical and basal dendritic spine densities were analyzed at P14, P21, and P35 (Figure 5C, D). Similar to dominant-negative nectin-3, overexpression of nectin-3 produced an overall decrease in dendritic spine densities when all time points were considered together (Figure 5E). Unlike dominant-negative nectin-3, a significant increase in spine densities was observed between P14 and P21 in nectin-3 overexpression neurons (Figure 3F). There was also a slight decrease in dendritic spine densities between P21 and P35, but this effect was not significant (Figure 3F). These data further support the conclusion that nectin-3 signaling at the synapse promotes spinogenesis between P14 and P21, but the increased synaptic adhesion produced by nectin-3 overexpression may limit runaway increases in spine density by producing fewer stronger synapses.

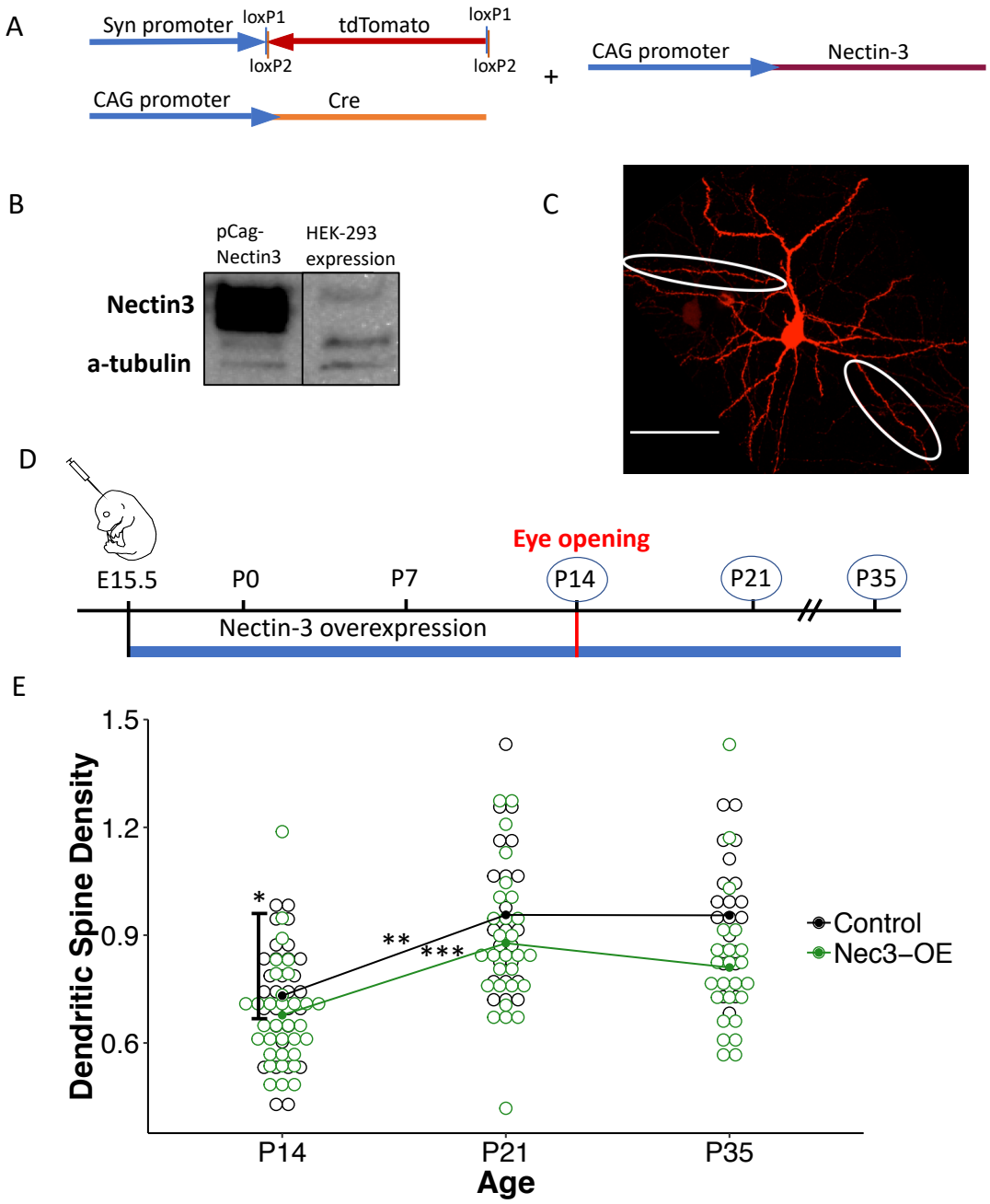

Figure 5: Nectin-3 overexpression at E15.5 produces an overall decrease in dendritic spine densities but facilitates synaptogenesis between P14 and P21.
(A) A nectin-3 expression construct was developed and co-electroporated into in developing L2/3 neurons with a Cre-dependent tdTomato construct and a Cre-expression plasmid.
(B) Western blot showing transfection of HEK-293 cells with a nectin-3 overexpression vector leads to greatly increased expression relative to endogenous nectin-3 levels.
(C) Representative image of an electroporated neuron with select apical and basal dendrites circled (scale bar = 50 µm).

(C) Nectin-3 overexpression constructs were introduced to L2/3 cortical neurons by *in utero* electroporation at E15.5. Dendritic spine densities were measured at three time points: eye opening (P14), one week after eye opening (P21), or at the closing of the critical period for ODP (P35).
(E) Nectin-3 overexpression produced an overall decrease in dendritic spine densities compared to control (scramble shRNA) neurons (P = 0.0193). However, spine densities significantly increased between P14 and P21 (P = 0.0001), indicating synaptogenesis was intact. Apical and basal dendrites are pooled in this analysis. Significance is denoted by '*', and P-values are listed in Supplemental Table 1.

Spine densities on apical and basal dendrites demonstrate different patterns of developmental change considering control, nectin-3 loss of function, and nectin-3 overexpression conditions

Neurons in visual cortex have been shown to experience intense synaptogenesis following eye opening[4,5]. This period of synapse formation (P14-P21 in mouse) is followed by the critical period for optical dominance plasticity (P21-P35), which is associated with synaptic refinement and pruning[4,7]. When nectin-3 manipulation was initiated at E15.5, the largest differences in dendritic spine densities between control (scramble shRNA), Nec3-shRNA, Nec3-DN, and Nec3-OE neurons was observed at P21 (Figure 6A, Supplemental figure 1). This result indicates that nectin-3 has a role in synaptogenesis following eye opening[4]. All conditions except Nec3-DN demonstrated a significant increase in spine densities from P14 to P21, consistent with previous studies examining synapse formation at this time[4]. When apical and basal dendrites are considered together, no significant differences are observed in dendritic spine densities between P21 and P35, though the spine densities of Nec3-shRNA and Nec3-OE neurons show a downward trend between these time points. Figure 6B provides a summary of these results, and shows significant developmental trends described in previous sections (Figures 2, 4, and 5).

Basal and apical dendrites had different developmental trajectories for spine formation, depending on the condition examined (Figure 6C, D). When basal dendrites are considered alone, significant increases in spine densities are observed between P14 and P21 for control, Nec3-shRNA, and Nec3-OE conditions. Dendritic spine densities for these three conditions also trended downwards between P21 and P35. While none of these trends are statistically significant when considered

individually, if all three conditions are grouped, a significant decrease in spine densities is observed. Nec3-DN was removed from this analysis since it prevented developmental spinogenesis after eye opening and therefore should not be used to estimate developmental changes in spine densities. This result indicates synapse pruning is occurring on basal dendrites between P21 and P35, though we acknowledge that the manipulation of nectin-3 expression in Nec3-OE and Nec3-shRNA neurons may have affected this result (Figure 6C).

When apical dendrites are considered alone, only Nec3-OE and Nec3-shRNA conditions show significantly increased spine densities between P14 and P21. Dendritic spine densities increased more slowly on the apical dendrites of control neurons and had significantly increased spine densities at P35 compared to P14 (Supplemental Table 1). Previously reported changes in dendritic spine densities on apical dendrites from L2/3 visual cortical neurons over the critical period for ODP have been inconsistent[7,47]. Differences in the way spine densities are counted and the location of the dendrite relative to the cell-body may account for these discrepancies[7,47]. Here we examined secondary apical dendrites that extended off the primary apical dendrite, which may have unique developmental trajectories for spine formation. For certain comparisons, apical and basal dendritic spine densities may have been differentially affected (P-values included in Supplemental Table 1). Regardless, these differences in apical and basal spine densities do not fundamentally change the outcome of these nectin-3 manipulations: decreasing nectin-3 caused increased spine densities, and overexpressing nectin-3, regardless of whether the protein had an intact C-terminus, reduced spine densities.

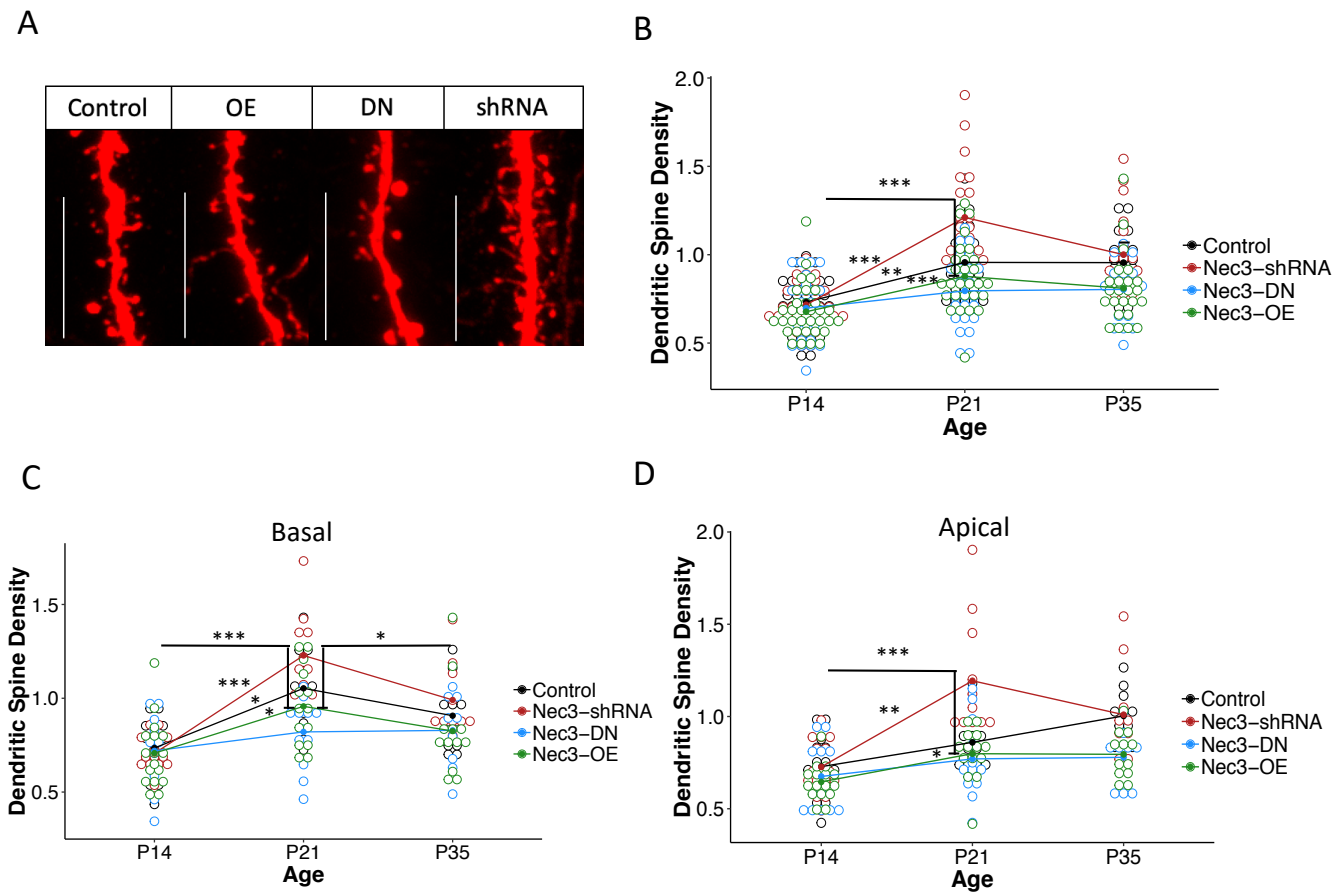

Figure 6: Apical and basal dendrites show different developmental trends in dendritic spine densities considering control, nectin-3 loss of function and nectin-3 overexpression conditions
(A) Images of representative dendrites from neurons electroporated at E15.5 with scramble shRNA (control), nectin-3 shRNA (shRNA), dominant-negative nectin-3 (DN), or full-length nectin-3 (OE) expression constructs and assayed at P21 (Scale bar = 15um).
(B) When apical and basal dendrites are pooled, all conditions except Nec3-DN show significant increases in spine densities from P14 to P21 (P-values listed in previous figures and Supplemental Table 1). This increase is highly significant when all conditions except Nec3-DN are considered together (P = < 0.0001). No significant differences in spine densities were observed between P21 and P35. Significance is denoted by '*', and P-values are listed in Supplemental Table 1.
(C) Developmental trends in dendritic spine densities considering only basal dendrites. All conditions except Nec3-DN show significant increases in spine densities between P14 to P21 when considered individually (control, P = 0.0209; Nec3-shRNA, P = 0.0002; Nec3-DN, P =0.5747; Nec3-OE, P = 0.0353). This increase is highly significant when all conditions except Nec3-DN are considered together (P = < 0.0001). A decrease in spine densities between P21 and P35 is trending for all conditions except Nec3-DN but is only significant if these three conditions are grouped and analyzed together (P = 0.0259). Significance is denoted by '*', and P-values are listed in Supplemental Table 1.
(D) Developmental trends in dendritic spine densities considering only apical dendrites. Only Nec3-shRNA and Nec3-OE show significant increases in spine densities between P14 and P21 (control, P = 0.3355; Nec3-shRNA, P = 0.0044; Nec3-DN, P =0.5110; Nec3-OE, P = 0.0170). This increase is highly significant when all conditions except Nec3-DN are considered together. No significant pruning effect is

observed between P21 and P35 considering apical dendrites alone. Significance is denoted by '*', and P-values are listed in Supplemental Table 1.

Discussion

We examine the developmental changes in dendritic spine densities on L2/3 visual cortical neurons after manipulating nectin-3 expression levels *in vivo* using *in utero* electroporation. Consistent with previous studies of synapse formation after eye opening in visual cortex[4,48–51], we found dendritic spine densities on L2/3 neurons increased from P14 to P21 for all conditions except Nec3-DN. Following this period of synaptogenesis in visual cortex, synaptic refinement and pruning is thought to occur during the critical period for ocular dominance plasticity (P21-P35)[7,36,47,48,52,53]. However, we did not observe any significant decreases in dendritic spine densities between P21 and P35 when apical and basal dendrites were analyzed together[7,54]. When apical and basal dendrites were analyzed separately and data from multiple conditions was combined (excluding Nec3-DN, Figure 6), dendritic spine densities on basal dendrites, but not apical dendrites, significantly decreased between P21 and P35. These data indicate that apical and basal dendrites on L2/3 neurons may have different developmental trajectories for synapse formation and refinement in developing visual cortex.

While the critical period for ODP is commonly associated with synapse pruning, previous studies have not consistently observed decreases in dendritic spine densities during this time[5,7,47]. This inconsistency is likely due to variability in methods of spine counting, the types of dendrites analyzed, the ages of animals assayed, the laminar locations of neurons analyzed, or differences in model organism[5,7,47,48,55]. One study found the spine densities on apical dendrites from L2/3 and L5 visual cortical neurons were highly variable and increased slightly between P20 and P30[47]. Another study showed apical dendritic spine densities in L2/3 decreased between P23 and P30[7]. Since apical dendrites can receive different inputs depending on their location in the cortical column, it is possible that the

selection of different types of apical dendrites or different spine counting techniques could account for these discrepancies. More rigorous studies of dendritic spine densities on different types of dendrites and neurons during developmental critical periods are necessary to clarify this issue.

There are a number of challenges associated with using *in utero* electroporation to manipulate protein expression in developing neurons. Plasmid concentration in a given electroporated neuron can vary greatly, potentially leading to increased phenotypic variability from neuron to neuron within a single condition. In addition, there is high endogenous variability in spine densities between dendrites and cells in L2/3 visual cortex. We focused on apical and basal dendrites at least one branch away from the soma in order to limit the effect of this variability, however it was still difficult to obtain robust estimates of population differences. Furthermore, our results from this study indicate apical and basal dendrites may have different developmental trajectories, which may have further increased variability. However, most overall effects, including increased spine densities with nectin-3 knockdown and decreased spine densities with nectin-3 expression, were consistent between apical and basal dendrites. For this reason, we decided to combine apical and basal dendrites for most of our analyses, and we consider dendrite type (apical vs basal) as a fixed effect in our statistical models (see methods). We further believe combining both dendrite types provides a more accurate approximation of the overall cellular effect of nectin-3 manipulation.

Nectin-3 knockdown in adult hippocampus was previously shown to decrease dendritic spine densities relative to control[18,20]. In contrast, we show here that nectin-3 knockdown at E15.5 in L2/3 visual cortical neurons increased dendritic spine densities relative to control at P21, but not at P14 or P35. Differences between this and previous studies may be due to innate differences between hippocampal and cortical neuron function and regulation, or may explained by differences in the developmental stage of the neurons examined. Consistent with the latter, it was previously shown that

blocking nectin-1 and nectin-3 binding in developing cultured hippocampal neurons increased spine number concomitant with a decrease in spine size at 10 and 16 days in culture[14]. This increase in spine number was proposed to be compensatory for the decreased size/strength of individual synapses[14]. During the development of visual cortex, dendritic spine densities and the frequency of mEPSCs (an indicator of synapse number) increase in the week following eye opening[4]. This increase in synapse number occurs simultaneously with a decrease in mEPSC amplitude, an indicator of synaptic strength[4]. If decreased synaptic strength is a prerequisite to increase synapse number, it is possible that nectin-3 knockdown further facilitates the rapid increase in synapse number following eye opening by decreasing synaptic strength. Though we have no readout of synaptic strength in this study, spine densities from Nec3-shRNA neurons were not different from control at P35, indicating the extra spines formed at P21 may have been weaker and removed over the critical period for ODP.

By P35, neurons may have begun to compensate for the extended (beginning at E15.5) shRNA knockdown of nectin-3, reducing spine densities. We next wanted to examine the effects nectin-3 knockdown between P21 and P35 independent from previous developmental effects (increased spine density at P21). To accomplish this, we performed an additional experiment where our Cre-dependent nectin-3 shRNA construct was electroporated into cortical neurons at E15.5, and a CaMKII-Cre mouse was used to drive Cre expression in cortical neurons after eye opening. Cre/loxP recombination was first detected in the cortex and hippocampus of CamKII-Cre mice at P19, and was described as robust by P23[23]. From this, we concluded that the knockdown of nectin-3 likely occurred in most cells around the start of the critical period for ocular dominance plasticity (P21). When nectin-3 knockdown was initiated at this later developmental stage, spine densities were increased relative to control at P35, suggesting the extended knockdown of nectin-3 from E15.5-P35 caused compensatory pruning after P21. This result further indicates that nectin-3 mediated cell adhesion may have a role in either restricting spine

formation, as discussed above, or enhancing synapse pruning over the critical period for ocular dominance plasticity (P21-P35). It was previously demonstrated that competition between dendritic spines for N-cadherin may drive activity-dependent pruning in motor cortex[53]. One hypothesis is that the recruitment of N-cadherin by nectin-3 may facilitate spine pruning through the selective strengthening of active spines and competitive reduction of N-cadherin in inactive spines. In this way, nectin-3 binding may help with the spatiotemporal strengthening and weakening of specific connections by L2/3 cortical neurons over the critical period for ocular dominance plasticity in V1.

In certain contexts, decreased synaptic cell adhesion may increase synapse number either to compensate for reduced synaptic strength[14], or by allowing the redistribution of membrane components to sites where new synapses form[38]. We next wanted to determine whether the increase in dendritic spine densities observed after shRNA knockdown was a result of reduced nectin-3 adhesion (extracellular binding) or reduced nectin-3 signaling at synapses. To observe the effects of increased nectin-3 adhesion, with and without intracellular signaling, we performed two separate experiments overexpressing either full length nectin-3 or dominant-negative nectin-3 in developing L2/3 neurons beginning at E15.5. Both proteins had intact extracellular binding domains (cell-adhesion), but dominant-negative nectin-3 lacked its C-terminus (intracellular signaling)[29]. Both full-length and dominant-negative nectin-3 expression produced overall decreases in spine densities when all time points were considered together. This is consistent with a model whereby high levels of cell adhesion may be detrimental to the formation of new synapses after eye opening. Interestingly, however, only neurons expressing full length nectin-3 showed a significant increase in spine densities between P14 and P21. Expression of dominant-negative nectin-3 prevented this developmental increase in spine densities, indicating that when nectin-3 is present at synapses, it facilitates spine growth through intracellular signaling. This is consistent with other studies showing that signaling through nectin-3 leads to the

intracellular recruitment of N-cadherin/catenin complexes and activation of Cdc42 and Rac1 signaling pathways[10,14,41–44], which have known roles in synapse formation[45,46]. These results collectively indicate that the intracellular and extracellular domains of nectin-3 may have opposing effects during synaptogenesis after eye opening: the extracellular binding domain (adhesion) may restrict spine formation, while intracellular signaling may facilitate spine formation.

The study described here examines dendritic spine densities over the development of L2/3 visual cortical neurons after shRNA knockdown, dominant-negative expression, or overexpression of nectin-3. Differences in spine densities were described at three critical developmental time points in V1: P14 (eye opening), P21 (opening of the critical period for ODP), and P35 (close of the critical period for ODP). We were able to identify nectin-3 dependent changes in dendritic spine densities which became evident after eye opening and were dependent on time of knockdown and intracellular signaling. From these studies, we hypothesize that nectin-3 may have roles in the formation and strengthening specific synapses; preventing runaway spine formation at P21 and facilitating the selective removal of inactive spines between P21 and P35. Further experiments are necessary to validate these hypothesized roles for nectin-3 in cell-type specific spine formation and stabilization in L2/3 of visual cortex. Similar to the experiment performed in Bian et al., 2015, it would be informative to examine whether nectin-1 to nectin-3 binding at specific synapses in cultured neurons facilitates the competitive accumulation of cadherin/catenin complexes to those synapses and reduction at other synapses[53]. Electrophysiological recordings or calcium indicator imaging of neuronal activity could help determine whether nectin-3 expression facilitates the refinement of visual response properties (such as orientation selectivity, receptive field structure, or contextual modulation) in L2/3 cortical neurons, which would be expected if nectin-3 enables selective synaptic strengthening and pruning. Our study also did not address whether nectin-3 is regulated by activity, which could be determined by examining nectin-3 dependent effects on

spine density and synapse function after dark rearing. Though more work is necessary, we identify what may be a novel mechanism for the selective formation and strengthening of specific synapses through nectin-3 signaling in L2/3 visual cortical neurons.

References Cited

1. Hackett TA, Guo Y, Clause A, et al. Transcriptional maturation of the mouse auditory forebrain. *BMC Genomics*. 2015;16(1):606. doi:10.1186/s12864-015-1709-8

2. Dalva MB, McClelland AC, Kayser MS. Cell adhesion molecules: signalling functions at the synapse. *Nat Rev Neurosci*. 2007;8(3):206-220. doi:10.1038/nrn2075

3. Mower GD, Berry D, Burchfiel JL, Duffy FH. Comparison of the effects of dark rearing and binocular suture on development and plasticity of cat visual cortex. *Brain Res*. 1981;220(2):255-267. doi:10.1016/0006-8993(81)91216-6

4. Desai NS, Cudmore RH, Nelson SB, Turrigiano GG. Critical periods for experience-dependent synaptic scaling in visual cortex. *Nat Neurosci*. 2002;5(8):783-789. doi:10.1038/nn878

5. Chen M-Q, Bi A-L, Zhang Y-Y, et al. Different patterns of changes between actin dynamics and synaptic density in the rat's primary visual cortex during a special period of visual development. *Brain Res Bull*. 2017;132:199-203. doi:10.1016/J.BRAINRESBULL.2017.06.004

6. Flavell SW, Cowan CW, Kim T-K, et al. Activity-Dependent Regulation of MEF2 Transcription Factors Suppresses Excitatory Synapse Number. *Science (80-)*. 2006;311(5763):1008-1012. doi:10.1126/science.1122511

7. Vidal GS, Djurisic M, Brown K, Sapp RW, Shatz CJ. Cell-Autonomous Regulation of Dendritic Spine Density by PirB. *eNeuro*. 2016;3(5). doi:10.1523/ENEURO.0089-16.2016

8. Lin Y-C, Koleske AJ. Mechanisms of synapse and dendrite maintenance and their disruption in psychiatric and neurodegenerative disorders. *Annu Rev Neurosci*. 2010;33:349-378. doi:10.1146/annurev-neuro-060909-153204

9. Hoy JL, Niell CM. Layer-specific refinement of visual cortex function after eye opening in the awake mouse. *J Neurosci*. 2015;35(8):3370-3383. doi:10.1523/JNEUROSCI.3174-14.2015

10. Honda T, Sakisaka T, Yamada T, et al. Involvement of nectins in the formation of puncta adherentia junctions and the mossy fiber trajectory in the mouse hippocampus. *Mol Cell Neurosci*. 2006;31(2):315-325. doi:10.1016/J.MCN.2005.10.002

11. Rikitake Y, Mandai K, Takai Y. The role of nectins in different types of cell-cell adhesion. *J Cell Sci*. 2012;125(16):3713-3722. doi:10.1242/jcs.099572

12. Takai Y, Nakanishi H. Nectin and afadin: novel organizers of intercellular junctions. *J Cell Sci*. 2003;116(Pt 1):17-27. doi:10.1242/JCS.00167

13. Tachibana K, Nakanishi H, Mandai K, et al. Two cell adhesion molecules, nectin and cadherin, interact through their cytoplasmic domain-associated proteins. *J Cell Biol*. 2000;150(5):1161-1176. doi:10.1083/JCB.150.5.1161

14. Mizoguchi A, Nakanishi H, Kimura K, et al. Nectin: an adhesion molecule involved in formation of synapses. *J Cell Biol*. 2002;156(3):555-565. doi:10.1083/jcb.200103113

15. Lim ST, Lim K-C, Giuliano RE, Federoff HJ. Temporal and spatial localization of nectin-1 and l-afadin during synaptogenesis in hippocampal neurons. *J Comp Neurol*. 2008;507(2):1228-1244. doi:10.1002/cne.21608

16. Maurin H, Seymour CM, Lechat B, et al. Tauopathy Differentially Affects Cell Adhesion Molecules in Mouse Brain: Early Down-Regulation of Nectin-3 in Stratum Lacunosum Moleculare. Vitorica J, ed. *PLoS One*. 2013;8(5):e63589. doi:10.1371/journal.pone.0063589

17. van der Kooij MA, Fantin M, Rejmak E, et al. Role for MMP-9 in stress-induced downregulation of nectin-3 in hippocampal CA1 and associated behavioural alterations. *Nat Commun*. 2014;5:4995. doi:10.1038/ncomms5995

18. Wang X-X, Li J-T, Xie X-M, et al. Nectin-3 modulates the structural plasticity of dentate granule cells and long-term memory. *Transl Psychiatry*. 2017;7(9):e1228. doi:10.1038/tp.2017.196

19. Gong Q, Su Y-A, Wu C, et al. Chronic Stress Reduces Nectin-1 mRNA Levels and Disrupts Dendritic Spine Plasticity in the Adult Mouse Perirhinal Cortex. *Front Cell Neurosci*. 2018;12:67. doi:10.3389/fncel.2018.00067

20. Wang X-D, Su Y-A, Wagner K V, et al. Nectin-3 links CRHR1 signaling to stress-induced memory deficits and spine loss. *Nat Neurosci*. 2013;16(6):706-713. doi:10.1038/nn.3395

21. Tomorsky J, DeBlander L, Kentros CG, Doe CQ, Niell CM. TU-Tagging: A Method for Identifying Layer-Enriched Neuronal Genes in Developing Mouse Visual Cortex. *eNeuro*. 2017;4(5). doi:10.1523/ENEURO.0181-17.2017

22. ISH Data :: Allen Brain Atlas: Developing Mouse Brain. http://developingmouse.brain-map.org/. Accessed October 27, 2015.

23. Tsien JZ, Chen DF, Gerber D, et al. Subregion- and cell type-restricted gene knockout in mouse brain. *Cell*. 1996;87(7):1317-1326. doi:10.1016/S0092-8674(00)81826-7

24. Piscopo DM, Weible AP, Rothbart MK, Posner MI, Niell CM. Changes in white matter in mice resulting from low-frequency brain stimulation. *Proc Natl Acad Sci U S A*. 2018;115(27):E6339-E6346. doi:10.1073/pnas.1802160115

25. Oh SW, Harris JA, Ng L, et al. A mesoscale connectome of the mouse brain. *Nature*. 2014;508(7495):207-214. doi:10.1038/nature13186

26. Wehr M, Hostick U, Kyweriga M, et al. Transgenic silencing of neurons in the mammalian brain by expression of the allatostatin receptor (AlstR). *J Neurophysiol*. 2009;102(4):2554-2562. doi:10.1152/jn.00480.2009

27. Lein ES, Hawrylycz MJ, Ao N, et al. Genome-wide atlas of gene expression in the adult mouse brain. *Nature*. 2007;445(7124):168-176. doi:10.1038/nature05453

28. ISH Data :: Allen Brain Atlas: Mouse Brain. http://mouse.brain-map.org/. Accessed October 27, 2015.

29. Gil-Sanz C, Franco SJ, Martinez-Garay I, Espinosa A, Harkins-Perry S, Müller U. Cajal-Retzius Cells Instruct Neuronal Migration by Coincidence Signaling between Secreted and Contact-Dependent Guidance Cues. *Neuron*. 2013;79(3):461-477. doi:10.1016/j.neuron.2013.06.040

30. Ventura A, Meissner A, Dillon CP, et al. Cre-lox-regulated conditional RNA interference from transgenes. *Proc Natl Acad Sci U S A*. 2004;101(28):10380-10385. doi:10.1073/pnas.0403954101

31. Mahmood T, Yang PC. Western blot: Technique, theory, and trouble shooting. *N Am J Med Sci*. 2012;4(9):429-434. doi:10.4103/1947-2714.100998

32. Harwell CC, Parker PRL, Gee SM, et al. Sonic Hedgehog Expression in Corticofugal Projection Neurons Directs Cortical Microcircuit Formation. *Neuron*. 2012;73(6):1116-1126. doi:10.1016/J.NEURON.2012.02.009

33. Walantus W, Castaneda D, Elias L, Kriegstein A. In utero intraventricular injection and electroporation of E15 mouse embryos. *J Vis Exp*. 2007;(6). doi:10.3791/239

34. Paxinos G, Franklin K. *Paxinos and Franklin's the Mouse Brain in Stereotaxic Coordinates, Fourth Edition*. Academic Press; 2013.

35. Satoh-Horikawa K, Nakanishi H, Takahashi K, et al. Nectin-3, a new member of immunoglobulin-like cell adhesion molecules that shows homophilic and heterophilic cell-cell adhesion activities. *J Biol Chem*. 2000;275(14):10291-10299. doi:10.1074/JBC.275.14.10291

36. Espinosa JS, Stryker MP. Development and plasticity of the primary visual cortex. *Neuron*. 2012;75(2):230-249. doi:10.1016/j.neuron.2012.06.009

37. Katz LC, Shatz CJ. Synaptic activity and the construction of cortical circuits. *Science (80-)*. 1996;274(5290):1133-1138. doi:10.1126/science.274.5290.1133

38. Bailey CH, Chen M, Keller F, Kandel ER. Serotonin-mediated endocytosis of apCAM: an early step of learning-related synaptic growth in Aplysia. *Science*. 1992;256(5057):645-649. http://www.ncbi.nlm.nih.gov/pubmed/1585177. Accessed November 1, 2018.

39. El-Brolosy MA, Stainier DYR. Genetic compensation: A phenomenon in search of mechanisms. *PLoS Genet*. 2017;13(7):e1006780. doi:10.1371/journal.pgen.1006780

40. Sheppard D. Dominant negative mutants: tools for the study of protein function in vitro and in vivo. *Am J Respir Cell Mol Biol*. 1994;11(1):1-6. doi:10.1165/ajrcmb.11.1.8018332

41. Tanaka Y, Nakanishi H, Kakunaga S, et al. Role of nectin in formation of E-cadherin-based adherens junctions in keratinocytes: Analysis with the N-cadherin dominant negative mutant. *Mol Biol Cell*. 2003;14(4):1597-1609. doi:10.1091/mbc.E02-10-0632

42. Kawakatsu T, Ogita H, Fukuhara T, et al. Vav2 as a Rac-GDP/GTP exchange factor responsible for the nectin-induced, c-Src- and Cdc42-mediated activation of Rac. *J Biol Chem*. 2005;280(6):4940-4947. doi:10.1074/jbc.M408710200

43. Fukuhara A, Shimizu K, Kawakatsu T, Fukuhara T, Takai Y. Involvement of nectin-activated Cdc42 small G protein in organization of adherens and tight junctions in Madin-Darby canine kidney cells. *J Biol Chem*. 2003;278(51):51885-51893. doi:10.1074/jbc.M308015200

44. Ogita H, Takai Y. Activation of Rap1, Cdc42, and Rac by Nectin Adhesion System. In: *Methods in Enzymology*. Vol 406. ; 2006:415-424. doi:10.1016/S0076-6879(06)06030-7

45. Brusés JL. N-cadherin signaling in synapse formation and neuronal physiology. *Mol Neurobiol*. 2006;33(3):237-252. doi:10.1385/MN:33:3:237

46. Duman JG, Mulherkar S, Tu YK, X. Cheng J, Tolias KF. Mechanisms for spatiotemporal regulation of Rho-GTPase signaling at synapses. *Neurosci Lett*. 2015;601:4-10. doi:10.1016/j.neulet.2015.05.034

47. de Vivo L, Faraguna U, Nelson AB, et al. Developmental Patterns of Sleep Slow Wave Activity and Synaptic Density in Adolescent Mice. *Sleep*. 2014;37(4):689-700. doi:10.5665/sleep.3570

48. Zuo Y, Lin A, Chang P, Gan W-B. Development of long-term dendritic spine stability in diverse regions of cerebral cortex. *Neuron*. 2005;46(2):181-189. doi:10.1016/j.neuron.2005.04.001

49. Cruz-Martín A, Crespo M, Portera-Cailliau C. Delayed stabilization of dendritic spines in fragile X mice. *J Neurosci*. 2010;30(23):7793-7803. doi:10.1523/JNEUROSCI.0577-10.2010

50. Chen C-C, Lu J, Zuo Y. Spatiotemporal dynamics of dendritic spines in the living brain. *Front Neuroanat*. 2014;8:28. doi:10.3389/fnana.2014.00028

51. Blue ME, Parnavelas JG. The formation and maturation of synapses in the visual cortex of the rat. I. Qualitative analysis. *J Neurocytol*. 1983;12(4):599-616. http://www.ncbi.nlm.nih.gov/pubmed/6619906. Accessed October 31, 2018.

52. Huang X, Stodieck SK, Goetze B, et al. Progressive maturation of silent synapses governs the duration of a critical period. *Proc Natl Acad Sci U S A*. 2015;112(24):E3131-E3140. doi:10.1073/pnas.1506488112

53. Bian WJ, Miao WY, He SJ, Qiu Z, Yu X. Coordinated Spine Pruning and Maturation Mediated by Inter-Spine Competition for Cadherin/Catenin Complexes. *Cell*. 2015;162(4):808-822. doi:10.1016/j.cell.2015.07.018

54. Benoit J, Ayoub AE, Rakic P. Transcriptomics of critical period of visual cortical plasticity in mice. *Proc Natl Acad Sci U S A*. 2015;112(26):8094-8099. doi:10.1073/pnas.1509323112

55. Juraska JM. The development of pyramidal neurons after eye opening in the visual cortex of hooded rats: A quantitative study. *J Comp Neurol*. 1982;212(2):208-213. doi:10.1002/cne.902120210